An Improved Gas Electron Diffractometer – The Instrument, Data Collection, Reduction and Structure Refinement Procedures

Raphael J. F. Berger, Manfred Hoffmann, Stuart A. Hayes, and Norbert W. Mitzel

Lehrstuhl für Anorganische Chemie und Strukturchemie, Universität Bielefeld, 33615 Bielefeld, Germany

Reprint requests to Prof. Dr. N. W. Mitzel. E-mail: mitzel@uni-bielefeld.de

Dedicated to Professor Hubert Schmidbaur on the occasion of his 75th birthday

The improvement of a Balzers Eldigraph KD-G2 gas-phase electron diffractometer, previously operated at the University of Tübingen, is reported. The diffractometer was equipped with a state-of-the-art telefocus electron gun, and high-energy radiation-sensitive imaging plates were introduced as detector system. A differential vacuum pumping system separating the diffraction chamber from the electron source was installed. A nozzle for the evaporation of compounds in a temperature range from 25 to 400 °C was constructed and its functionality proven by the structure determination of quinoline. Calibration, data reduction and structure refinement using standard procedures in connection with a selection of literature-known programs are described. The gas-phase structure of quinoline was determined, discussed and compared with *ab initio* and solid-state X-ray diffraction results.

Key words: Gas Electron Diffraction, Gas-phase Structure Determination, Structural Chemistry, Instrumentation, 2-Azabicyclo[4.4]dec-1,3,5,7,9-penta-en

Introduction

Following the discovery of the atomic and molecular nature of matter, chemistry's next big step towards an exact science was the elucidation of the geometrical structure of molecules. While the idea that matter is made up of atoms and molecules was considered long ago in ancient Greece [1], mankind had to wait until the early days of quantum mechanics for experimental evidence, when X-ray and electron-diffraction of crystalline and gaseous compounds were established [2, 3]. Even now, these two methods are the most direct ways of observing geometric relations between atoms in molecules. Compared to the ubiquitous X-ray diffraction facilities, gas electron diffraction (GED) is relatively rarely used as a source of structural information [4]. The predominant factor is the limited information content in a GED pattern, resulting from random orientation of molecules. However, the lack of commercially available equipment also plays a role, and it is the hope of the authors that a clear description of the experimental set-up and data handling might inspire others to venture into this field.

The current state-of-the-art in refinement procedures in most cases makes some use of the results of *ab initio* calculations, thus the interaction of theoretical chemistry and GED is an example of a symbiotic coexistence of two quite different scientific disciplines. Since an exact solution of the basic quantum-mechanical equations describing the physics of molecular systems is still only possible for a vanishing number of examples, a major concern of theoretical chemistry is the choice of both, appropriate and feasible approximations. This choice often turns out to be critical, despite the rapid development of computational power, and is still a highly problematical task [5]. In this respect, reliable experimental data are at least comforting, and at times vital for the validation of the chosen approximations and methods.

With respect to GED, one generic limitation is the amount of information that can be derived from electron scattering data of gases. Structure determinations using only GED data are restricted to a comparably small number of compounds comprising small or highly symmetrical molecules. In order to determine molecular gas-phase structures of more complicated compounds by GED it is necessary to include additional information into the refinement, and to make assumptions about global or local symmetry or about geometric parameters or more often a combination of

these. Different procedures are described in the literature for making use of non-GED structure information from *ab initio* calculations [6, 7], spectroscopy (*e. g.* MW) [8] or molecular dynamics calculations [9]. *Vice versa*, a comparison of GED data with computationally or spectroscopically derived data may serve as a test for the reliability of a structure refinement.

The interaction of these disciplines allows direct access to the geometry of free molecules, unbiased from intermolecular interactions. In many cases, the intrinsic differences between gas-phase and solid-state structures of the same (molecular) compound are substantially larger than the accuracy of the nowadays available standard methods of computation [10 – 18]. Thus, when a crystal structure is available, it is of interest to compare the gas- and solid-state structures, as well as the results of experiment and theory. In this respect GED is the central technique, able to discern the source of disagreements between crystal structures and the results of *first principles* calculations on isolated molecules.

Since the main parts of the Bielefeld GED instrument were constructed in the late 1960's, one aspect of our work has been to catch up with the latest instrumental developments and techniques applicable in a gas-phase electron diffractometer. In this report we describe the changes in the experimental set-up, and the details of the data collection, reduction and structure refinement process, which we apply in the standard structure determination procedure.

Results and Discussion

The original design and set-up of Balzers KD-G2 [19] closely resembles the Trüb&Täuber electron microscope KD3 [20] with the exception of the gas nozzle, the cold trap and the plate-changing mechanism. The main construction plan is displayed in Fig. 1, a photograph of the whole system in Fig. 2, and a detail of the part for manipulating size and direction of the electron beam is shown in Fig. 3.

Vacuum system

In contrast to the original setup, the pumping system of the electron gun was separated from the pumping system of the diffraction chamber. The two parts are connected with a pneumatically operated shutter valve. The two independent vacuum chambers are moreover separated by a tube-like aperture of 3 mm diameter, close to a magnetic lens situated at the connection to
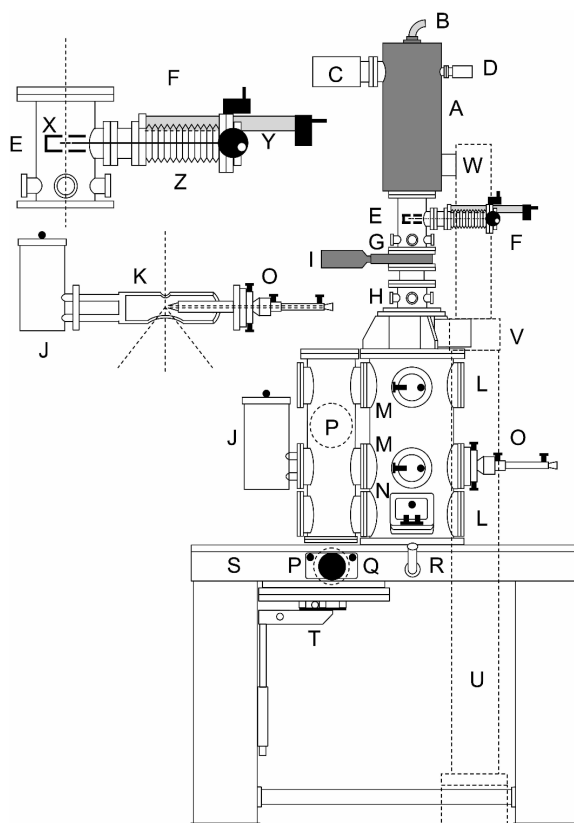

Fig. 1. Scheme of the GED instrument in Bielefeld including details of the apperture manipulator unit and the nozzle/cold trap assembly. **A** electron source, **B** high-voltage cable, **C** turbo molecular pump, **D** ion gauge, **E** aperture unit, **F** vacuum manipulator unit, **G** upper deflection unit, **H** lower deflection unit, **I** pneumatic shutter valve, cold trap: **J** N_2 reservoir, **K** copper cylinder of the cold trap supplied with liquid N_2, **L** flanges for long, and very short nozzle-plate distance assembly of the nozzle/cold trap unit, **M** upper lead glass windows, **N** lower lead glass window, **O** nozzle unit for sample evaporation inserted in the short-distance flange, **P** and **Q** control lamps for the positioning of the detector plates (small circles) and plate movement wheel (movement mechanism and plate not shown), **R** microscope (8 ×) for beam shape observation, **S** detection plane governing the rotation sector (not shown), **T** detector casette mounting unit (detector cassette with plates not shown), **U** hydraulic telescope cylinder, **V** anker connecting **U** with the main chamber, **W** anker connecting **U** with **A**, **X** Mo shielding cylinder (bold) and apperture holder with apperture (inside), **Y** adjustment nuts, **Z** steel bellow.

the diffraction chamber. As a consequence, pressure differences of about three orders of magnitude between the diffraction chamber and the electron gun can be maintained under dynamic vacuum with an open shutter valve. In this way, the filament and also the metal

Fig. 2. Photograph of the gas electron diffractometer at the University of Bielefeld.
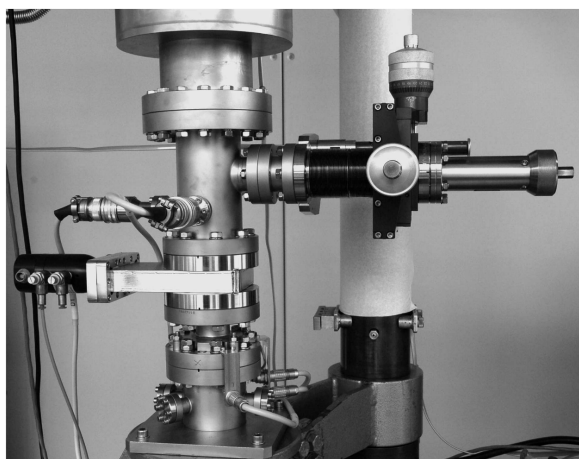

Fig. 3. Section of Fig. 2 showing (top to bottom) apperture manipulator, upper deflection unit, shutter valve and lower deflection unit as schematically shown in Fig. 1.

and insulator surfaces inside the electron source are protected from contamination with sample material or

other contaminants. Additionally, the pneumatic shutter valve can be closed instantaneously and during critical steps of the experiment, for instance sample degassing. The electron gun is pumped by an Edwards HDX24 turbo molecular pump (3.6 m^3/h), which is fore-pumped by an oil-free Edwards 5DX scroll pump. The original Trüb&Täuber rotary pump (45 m^3/h), used for the rough-pumping of the whole instrument as well as for fore-pumping the diffusion pump, was replaced by an Edwards EM80 rotary pump (80 m^3/h).

Detection system

Instead of using photographic plates as a detection system, reusable and high-vacuum-compatible, high-energy radiation-sensitive imaging plates from Fuji (BAS-IP MP 2025) are used. The radiation-sensitive material consists of Eu^{2+}-doped BaFBr. The exposed plates are scanned with a commercially available IP-Scanner (Fuji BAS 1800II). Imaging plates have a considerably larger dynamic range than photographic plates, reducing the criticality of the exposure, and produce intensity data of superior quality [21].

Electron source

The electron source was designed and manufactured by STAIB Instruments / Langenbach (Germany). It is based on a modification of the telefocus (Steigerwald) design. In addition to the Wehnelt cap it contains a second cylinder, which is insulated with respect to the filament. This enables the main focal plain of the electron beam to be varied, without changing the relative positions of the anode and cathode (filament). The grid (Wehnelt cap) potential ranges up to −1000 V with respect to the filament potential at most, while the focus (Wehnelt cylinder) potential ranges from 90 to 100 % of the total voltage with respect to the ground (anode) potential. Finger tip-type (Siemens) tungsten filaments of 100 μm diameter are used. This Wehnelt cap has a cone angle of 140°. The electron source is equipped with 8 deflection coils located at two different main positions, above and below the lens allowing an accurate positioning of the electron beam. In each of the two main deflection positions there are again upper and lower deflectors for both the *x* and *y* directions. The first deflection position is 150 mm below the filament and the second one is close to the electromagnetic lens at the outlet of the electron source. Between the first deflection plane and the filament, an *xyz*-manipulator for insert-
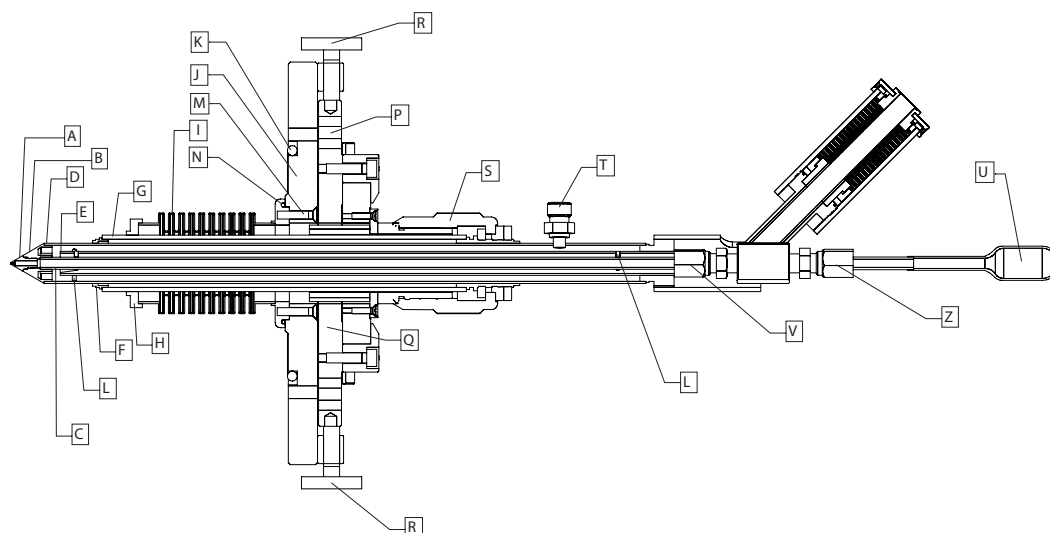
Fig. 4. Cross-sectional view of the newly-constructed GED nozzle system for sample temperatures up to 400 °C. For description and labels, see text.

ing apertures into the primary beam is mounted. 200, 100 and 50 μm platinum apertures are used. Using the 100 μm aperture usually more than 75 % of the primary beam current at optimum grid/focus-voltage and filament-current settings is maintained. The formerly mentioned electromagnetic lens is used for the focusing of the electron beam with respect to the detector plane as well as to defocus the electron beam to cast a shadow of the nozzle tip providing a simple and reliable method for positional adjustments of the gas inlet. The high-voltage power supply from Glassman Instruments (model WR100N2.5) generates a potential of up to 100 kV and up to 2.5 mA emission current. For standard measurements 1 – 5 μA emission current is an approximate upper limit. For certain purposes, such as compounds with very low vapour pressure, much higher beam currents can be achieved but at the cost of a wider beam diameter. The power supply has a facility that generates a voltage on the scale 0 to 10 V, that is in proportion to the generated high voltage. Thus, the stability of the high voltage may be monitored during the course of an experiment and has been found to vary by less than one or two volts during the course of the experiment.

The medium-temperature nozzle

For the purpose of GED measurements at elevated temperatures, up to 400 °C, an air-heatable nozzle was constructed (Fig. 4). Pressurised air (8 bar) is heated using a 1600 Watt tubular heating element manufactured by Hawco co. The construction is based on three concentric stainless-steel tubes **C** (6 mm outer diameter), **E** and **D** being soldered to the conical cooper element **B** (nozzle collet). The contact of **B** to **C** was first soldered, followed by the contact of **B** to **D**, with working temperatures for the solder at the **B/C** junction of 810 and at the at the **B/D** junction of 660 °C. Tube **E** is used to guide the hot air and to direct the exhaust of air into the sample reservoir. It is shortened by 5 mm in order to allow for taking up the nozzle collet **B**. Flange **J** bears the nozzle unit, which during the experiment is bolted to the main vacuum chamber. The guiding plates, **P** and **Q**, behind **J** are adjustable in the *x* and *y* directions, where the *xy* plane is orthogonal to the nozzle shaft. In this way the nozzle tip can be positioned relative to the electron beam *via* adjustment of the knurled screws **R** and **O** (not visible in Fig. 4). The adjustment nut **S** is used to position the nozzle tip in *z* direction. Hot air is introduced *via* the inlet **T** into the space between tubes **D** and **E** (*z* direction) and further on between tube **E** and tube **C** (-*z* direction). At the outlet between tubes **C** and **E** the exhaust air heats the sample. In this way it is ensured, that the nozzle tip is warmer than the sample. Usually, a temperature gradient of 10 to 20 K between **A** and **U** is easily established. Vacuum sealing positions are as follows: one O-ring **K**, which is thermally largely isolated from the inner tubes and mounted directly to the steel core of the main chamber; one PTFE O-ring **M** between the bolted

brass disc **N** and plate **J**, which is as also thermally well insulated from the inner tubes; the solder connection between the brass flex bellow **I** and the brass disc around **M**; the solder connection between **I** and **H**, the weld between **H** and **G**; the weld between **G** and **F**; the solder connection between **B** and **D**; the solder connection between **B** and **C**; the swage lock® connection between **W** and **C** and the consequent swage lock® connections to the sample ampule **U** containing a metal-glass transition. **B** has a thread which allows the use of different nozzle tips, **A**. Currently, a knife-edged aluminium tip with a bore of 0.75 mm is used. The cone angle of the tip (and the collet) is 60°.

Thermocouple wires (type K) fixed at **B**, **V** and **U** enable the measurement of the temperature distribution along the inner tube **C** and the sample reservoir **U**. The thermocouple wire from **B** is placed between the tubes **C** and **E**, hence no additional vacuum feedthrough was necessary, but the wire had to be fixed before soldering the connections to **B**.

Standard experimental conditions and parameters

During the measurements (using the N_2-cooled cold trap) we typically maintain background pressures of about 2×10^{-7} mbar with closed tap and 8.0×10^{-6} to 2.0×10^{-5} mbar whilst introducing the sample. The pressure in the electron source rises from 9.0×10^{-9} mbar with cold filament to 1×10^{-7} mbar during emission. In general measurements are carried out at an accelerating voltage of 60 kV and a filament current of 1.5 to 1.7 A. Grid and focus voltages have to be adjusted in order to optimise the ratio of primary beam current to net beam current in the diffraction chamber. This implies a focusing of the primary beam onto the plane of the apertures. For standard measurements a $100 \, \mu$m aperture is used near the source, and the magnetic lens is used to focus the beam onto the plane of the detection system. Typically, net beam currents of $100 \, n$A are employed. Under these conditions, the optically determined diameter of the light spot on a YAG single-crystal screen is about $120 \, \mu$m.

Standard measurements are carried out at two different nozzle-to-plate distances for each compound (250 and 500 mm). The exposure times vary under such conditions between 10 and 90 s depending on this distance (long distance – short exposure time) and on the scattering cross-section of the compound. The rotating sector is spun at a rate of $2 - 3$ Hz during the exposures.

Data reduction and structural refinement

The exposed imaging plates are scanned immediately after the experiment. For data reduction T. G. Strand's program PIMAG [22] is used, which is designed for reducing Fuji BAS 1800 scanner data to molecular scattering intensities. The 16-bit intensity values, J, read out from the scanner are converted by PIMAG into electron doses values, ED, using the formula:

$$ED = \frac{1}{4} \times 10^{\frac{5(J-2^{15})}{2^{16}-1}},$$

yielding doses values between 0 and approximately 79.1. The linearity of this function with respect to the applied dose was tested by exposing image plates to a ^{14}C source for a range of exposure times, spanning 0.5 min to 2.5 d. In this way, the random errors in the recorded intensities were found to be greater than any deviation from linearity of the applied function. The relative scaling of the two scanning directions is calibrated using an exposed image plate with two pairs of pin holes, which are scanned in two orientations, approximately perpendicular to one another. PIMAG governs also the sector correction, which requires a binary sector file in the format "$x_1 \, y_1 \, x_2 \, y_2 \, \ldots$" for x_i being the distance in mm from the sector centre at the sector plane and y_i being the respective sector opening angle in degrees. Currently, an averaged sector function is used, reconstructed from experimental xenon scattering data at 250 and 500 mm nozzle-to-plate distances, respectively.

Prior to the sample measurement, at least one reference data set is recorded in order to allow for the calibration of the instrument constant (ratio of electron wavelength to distance from the nozzle tip to the detection plate). Benzene is used as reference standard. The calibration procedure is carried out using the program ed@ed [23], which is also used for the structural refinement procedure.

Exemplary structure determination of quinoline structure model and refinement

Planarity (point group C_s) was assumed for the quinoline structure. Hence $(2 \times 17) - 3 = 31$ degrees of freedom have to be accounted for in a complete set of internal coordinates. Fig. 5 shows the set of internal coordinates chosen for the description of the molecular geometry and the atom numbering scheme used.
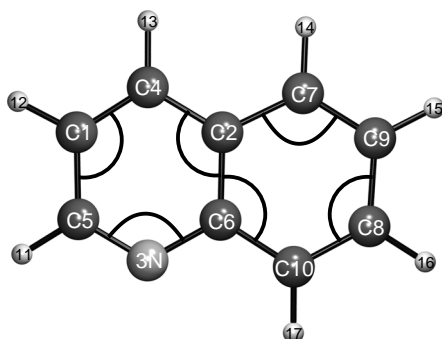
Fig. 5. Structure, atom numbering scheme and internal coordinates for the refinement of the gas-phase electron diffraction structure of quinoline. Each black line denotes an interatomic distance and each arc denotes an angle used as internal coordinate. All terminal atoms are hydrogen atoms.

In addition to the 18 interatomic distances, corresponding to all covalent bonds occurring in the molecule, and the six depicted C-C-C (and C-N-C) angles, for each hydrogen atom the differences between the two corresponding outer angles C-C-H (angular deviation of the C-H vector from the C-C-C bisector) were used for the description of the hydrogen atom positions.

A set of linear combinations of these internal coordinates were used as parameters p_i for the least-squares refinement using the programme ed@ed. The shorter heavy-atom interatomic distances $r_{3,5}, r_{3,6}, r_{1,4}, r_{7,9}$ and $r_{8,10}$, were grouped together ($r_1^s, \ldots, r_5^s$), as well as the slightly longer ones $r_{2,4}, r_{5,1}, r_{2,6}, r_{2,7}, r_{8,9}$ and $r_{6,10}$ ($r_1^l, \ldots, r_6^l$). In a similar way the six carbon backbone angles $w_{1,4,2}, w_{1,5,3}, w_{2,6,3}, w_{6,2,7}, w_{7,9,8}$ and $w_{8,10,6}$ are labeled ($w_1, \ldots, w_6$). A series of differences $\Delta^j r_i$ between the coordinates of one group can be defined (for instance for the five shorter distances r_i^s):

$$
\begin{aligned}
\Delta^0 r_i^s &= r_i^s, & i &\in 1,\ldots,5 \\
\Delta^1 r_i^s &= r_{i+1}^s - r_i^s, & i &\in 1,\ldots,4 \\
\Delta^2 r_i^s &= \Delta^1 r_{i+1}^s - \Delta^1 r_i^s, & i &\in 1,2,3 \\
\Delta^3 r_i^s &= \Delta^2 r_{i+1}^s - \Delta^2 r_i^s, & i &\in 1,2 \\
\Delta^4 r_1^s &= \Delta^3 r_2^s - \Delta^3 r_1^s
\end{aligned}
$$

The arithmetic mean of the zero-order difference series $\Delta^0 r_i^s$ is simply the arithmetic mean of all shorter interatomic distances, while the arithmetic mean of the first order differences $\Delta^1 r_i^s$ will reflect the broadness of the distribution. For consistency, the averages of the other higher-order difference series were formed, and all parameters were expressed in terms of their means

of the nth-order difference series:

$$
\overline{\Delta^i r} = \frac{1}{N-i} \sum_{j=1}^{N-i} \Delta^i r_j
$$

Since the average $\overline{\Delta^0 r^s}$ ($= \overline{r^s}$) of the shorter distances r_i^s and the average $\overline{\Delta^0 r^s}$ ($= \overline{r^l}$) of the longer distances r_i^l are on all levels of theory relative close-by an even weighted average and a difference were formed displaying the first two parameters for the refinement:

$$
p_1 = \frac{\overline{r^l} + \overline{r^s}}{2} \quad p_2 = \frac{\overline{r^l} - \overline{r^s}}{2}
$$

All other parameters were defined to be the averages of the difference sequences of the three parameter groups ($p_3 = \overline{\Delta r^s}$, $p_4 = \overline{\Delta^2 r^s}$, $p_5 = \overline{\Delta^3 r^s}$, $p_6 = \overline{\Delta^4 r^s}$, $p_7 = \overline{\Delta r^l}$, $p_8 = \overline{\Delta^2 r^l}$, $p_9 = \overline{\Delta^3 r^l}$, $p_{10} = \overline{\Delta^4 r^l}$, $p_{11} = \overline{\Delta^5 r^l}$, $p_{12} = \overline{w}$, $p_{13} = \overline{\Delta w}$, $p_{14} = \overline{\Delta^2 w}$, $p_{15} = \overline{\Delta^3 w}$, $p_{16} = \overline{\Delta^4 w}$, $p_{17} = \overline{\Delta^5 w}$). As a starting point for the refinement, the interatomic distances r_i^s and r_i^l and r_{CH} as well as the heavy atom angles w_i and the angle differences between the C-C-H angles from the calculations at the MP2/TZVPP level of theory were chosen. The distance parameters p_1, p_2, p_3, p_4 and the heavy atom angle parameters p_{12} and p_{13} could be refined unrestrained, while the distance parameters p_5, p_7, p_9, p_{10}, and p_{11} as well as the angular parameters p_{12} and p_{13} were restrained according to the averages and standard deviations from a series of calculations at a hierarchy of nine different levels of theory (HF/MP2/SCS-MP2//TZVP/TZVPP/ QZVPP). Moreover $r_{6,10}$ was also restrained to the average and the standard deviation of the computational values. The C-H ($p_{18} - p_{24}$) distances were set to the calculated average value, and a common scaling factor was introduced and refined independently. The angular deviations of the C-H vectors from the C-C-C/N bisectors $p_{25} - p_{31}$, were set to the values of the well-balanced MP2/TZVPP level of theory. Starting values for the vibrational amplitudes (u_{h1}) and corresponding harmonic distance corrections (k_{h1}) were generated from a harmonic force field (calculated at B3LYP/6-311G** level of theory) using the program SHRINK [24]. Five groups of interatomic vibrational amplitudes were refined together by means of a common scaling factor: all single-bonded C-H vibrations, all single-bonded heavy atom vibrations, all two-bond distant heavy-atom-H vibrations, all two-bond distant heavy-atom vibrations, and the remaining vibrational
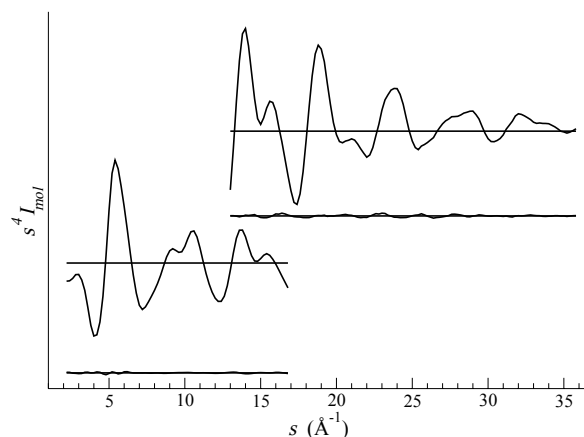
Fig. 6. Experimental and difference (experimental miuns theoretical) molecular-intensity curves for quinoline.

Fig. 7. Experimental and difference (experimental miuns theoretical) weighted radial-distribution function for quinoline. Molecular scattering intensities were multiplied by $s \exp(-3s^2\, 10^{-5}/[(Z_N - f_N)(Z_C - f_C)])$ prior to Fourier inversion. f_N and f_C denote the atomic scattering factors for nitrogen and carbon taken from ref. [25].

amplitudes. These five scaling factors were refined unrestrained.

The final experimental and difference molecular-intensity curves are shown in Fig. 6, while those for the radial distribution are shown in Fig. 7, and the final electron diffraction structure parameters (r_{h1}, R_D = 4.7 %, R_G = 6.4 %) are given in Fig. 8. Experimental conditions, selected vibrational amplitudes, a parameter correlation matrix and Cartesian coordinates of the final model are given in the Experimental Section.

On the gas-phase structure of quinoline

The GED structure determination of quinoline is a challenging but also rewarding undertaking. Depending on the smallest number of covalent bonds between all non-hydrogen atom pairs in a quinoline molecule, these atom pairs are partitioned into sets of almost equidistant pairs (one-bond distant, two-bond distant,..., five-bond distant atom pairs). Hence these distances are strongly correlated in terms of the diffraction intensity they cause, which is usually a major obstacle for an independent refinement of such structure parameters. On the other hand, all critical experimental parameters such as sample purity or partial pressure [26] can easily be controlled. Moreover the diffraction pattern of quinoline shows clearly distinct and contrasted fringes over the whole *s*-range of investigation (1.5 – 35.0 Å^{-1}), ensuring a high signal-to-noise ratio in the recorded intensities. Accurate computational structures are accessible for this comparably small, symmetric, single reference system. And last but not least in 2001 a solid-state X-ray structure of quinoline
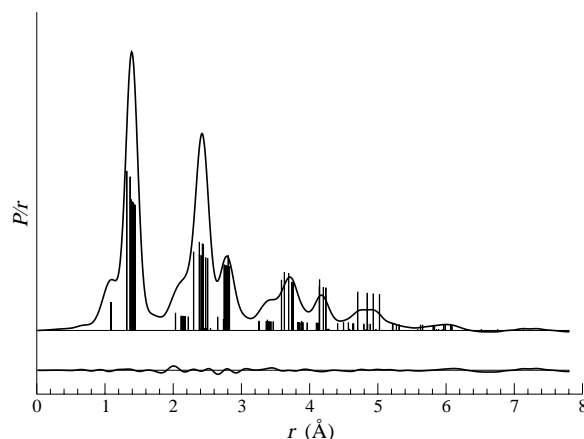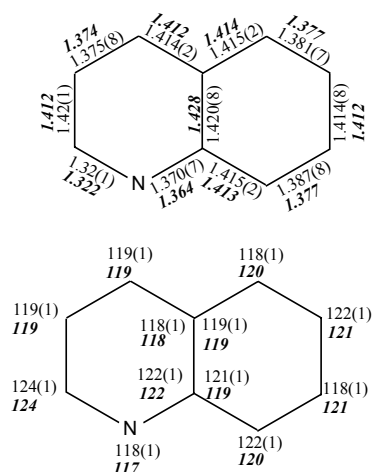

Fig. 8. MP2/TZVPP (bold italics) and experimental (r_{h1}) geometrical parameters of quinoline. Bond lengths in the upper diagram are given in Å units and inner angles in the lower diagram are given in degrees.

was described which can be also compared to the gas-phase results [27].

Fig. 8 gives an overview about the refined gas-phase structural parameters and in Table 5 the corresponding parameters from the solid-state structure are listed. All three methods show five shorter non-hydrogen-atom bonded distances (C5–N3, N3–C6, C4–C1, C9–C7, C10–C8) and six longer ones (the remaining). While for C5–N3 and N3–C6 this is explained due to the nitrogen atom which is involved as a bonding part-

Table 1. Experimental conditions (camera distances, nozzle and sample temperatures), data intervals, data ranges and trapezoidal weighting function points, correlation parameters, scale factors, electron wavelengths and final R factors for the GED experiments and refinements of quinoline.

Camera dist. (mm)	T_{samp} (°C)	T_{nozz} (°C)	Δs (Å^{-1})	Weighting function (Å^{-1})				Corrn. par.	Scale factor	Wavelength (Å)	R_G (%)	R_G tot. (%)	R_D (%)	R_D tot. (%)
				s_{min}	s_{w1}	s_{w2}	s_{max}							
501.88	102	112	0.2	2.2	4.2	14.6	17.0	0.4463	0.75(1)	0.04810	14.3		10.2	
250.00	105	114	0.2	13.0	15.0	30.8	35.8	0.4941	0.74(3)	0.04810	5.5	6.3	3.4	4.7

Table 2. Refined values of independent parameters including one standard deviation (e. s. d.), and respective restraints including used error estimate (e. s. d.), from *ab initio* calculations. r are all 11 bonded C-C and C-N distances, respectively; r^s are the 5 shortest distances of r; r^l are the remaining longer distances; w are the six independent C-C-C/N angles.

Par.	Value (e. s. d.)	Restraint (e. s. d.)	Description
p_1	1.3926(8)	–	mean of r $(=\overline{r})$
p_2	0.0261(38)	–	$(\overline{r^l} - \overline{r^s})/2$
p_3	0.0185(39)	–	mean of differences of r^s $(=\overline{\Delta r^s})$
p_4	−0.0174(61)	–	mean of 2nd order differences of r^s $(=\overline{\Delta^2 r^s})$
p_5	0.0223(67)	0.0231(81)	$\overline{\Delta^3 r^s}$
p_6	−0.047(21)	−0.021(3)	$\overline{\Delta^4 r^s}$
p_7	0.0002(1)	0.0002(1)	$\overline{\Delta r^l}$
p_8	−0.0010(28)	–	$\overline{\Delta^2 r^l}$
p_9	−0.0010(38)	−0.0043(44)	$\overline{\Delta^3 r^l}$
p_{10}	0.015(11)	0.0185(14)	$\overline{\Delta^4 r^l}$
p_{11}	0.028(92)	−0.14(13)	$\overline{\Delta^5 r^l}$
p_{12}	119.7(7)	–	$\overline{w}$
p_{13}	−0.05(30)	–	$\overline{\Delta w}$
p_{14}	−1.21(9)	−1.35(10)	$\overline{\Delta^2 w}$
p_{15}	1.888(50)	1.867(58)	$\overline{\Delta^3 w}$
p_{16}	−13.0(20)	−13.6(24)	$\overline{\Delta^4 w}$
p_{17}	1.0838(51)	1.0840(10)	$\overline{\Delta^5 w}$

Table 3. Independently refined reference amplitudes and corresponding distances including e. s. d.'s for the GED refinement of quinoline.

Atom pair	Distance (e. s. d., Å)	Amp. ref. (e. s. d., Å)	Amp. calcd. (e. s. d., Å)
H4-C13	1.082(5)	0.075(8)	0.0757
N3-C5	1.312(13)	0.049(6)	0.0427
N3···H17	2.035(11)	0.076(8)	0.0951
C6···C6	2.305(9)	0.047(6)	0.0515
C6···H11	3.264(12)	0.088(7)	0.0924

ner, the shortening of C4–C1, C9–C7, C10–C8 relative to the remaining distances can be explained by the degree of double bond character contained in these bonds, as can be predicted using valence bond theory. The bonding situation in quinoline is in this respect in full analogy to the bonding situation in naphthalene, showing four shorter C-C bonds and seven longer

Table 4. Correlation matrix elements ($\times$ 100) with absolute values $>$ 50 for the least-squares refinement of quinoline. k_1 and k_2 denote scaling factors.

	p_1	p_2	p_3	p_{10}	p_{12}	p_{13}	p_{24}	u_{12}	u_{47}	u_{56}	u_{62}	k_1	k_2
p_1		−62											
p_2	100		−83		−51	50							
p_3		100				53							
p_8				65									
p_{12}										64			
p_{13}			100										
u_8								−90					
u_{12}							100					56	
u_{19}								58					
u_{33}										−69			
u_{37}									−80				
u_{94}													53
k_1											100	56	
k_2													100

Table 5. Selected structure parameters of quinoline determined by *ab initio* calculations, solid-state X-ray diffraction and gas electron diffraction. Atom labeling according to Fig. 5. Distances are given in Å and angles in degrees. The experimental values include e. s. d.'s of 1 σ.

Parameter	MP2 r_e	XRD[a]		GED[b] r_{h1}
$r_{5,3}$	1.322	1.319(2)	1.320(2)	1.32(1)
$r_{3,6}$	1.364	1.374(2)	1.367(2)	1.370(7)
$r_{4,1}$	1.374	1.350(3)	1.359(2)	1.375(8)
$r_{9,7}$	1.377	1.358(2)	1.360(2)	1.381(7)
$r_{10,8}$	1.377	1.365(2)	1.358(2)	1.387(8)
$r_{1,5}$	1.412	1.400(3)	1.406(2)	1.42(1)
$r_{8,9}$	1.412	1.410(2)	1.405(2)	1.414(8)
$r_{2,4}$	1.412	1.414(2)	1.411(2)	1.414(2)
$r_{6,10}$	1.413	1.412(2)	1.410(2)	1.415(2)
$r_{7,2}$	1.414	1.416(2)	1.410(2)	1.415(2)
$r_{6,2}$	1.428	1.413(2)	1.418(2)	1.420(8)
$w_{6,3,5}$	117.3	117.0(1)	117.0(1)	118(1)
$w_{3,5,1}$	124.3	125.5(2)	124.6(1)	124(1)
$w_{5,1,4}$	119.0	119.0(2)	118.7(2)	119(1)
$w_{1,4,2}$	119.0	119.8(2)	119.4(2)	119(1)
$w_{4,2,6}$	118.2	117.3(2)	117.7(7)	118(1)
$w_{2,6,3}$	122.8	122.4(1)	122.5(1)	122(1)

[a] 150(2) K, two independent molecules were found in the asymmetric unit [27]; [b] 386(1) K, this work.

bonds, in accordance with the frequency of occurrence of double bonds in the three possible resonance structures [28].

As expected, the independent heavy atom angles show only a slight deviation from 120° in all angles involving nitrogen.

In general there is a good agreement between the gas-phase and the solid-state structure. However, standard deviations are higher for the gas-phase structural parameters (by about a factor of 4–5), and also a small systematic deviation towards shorter distances in the solid state [factor 0.993(6)] can be observed. This might be assigned to the difference between an approximate equilibrium structure (r_{h1} type) in GED and the thermally averaged reciprocal lattice positions, being determined in a X-ray diffraction solid-state structure [7].

The structural parameters from the MP2 calculation are almost all within the 1 σ interval of the corresponding gas-phase parameters (except $r_{10,8}$). This indicates that the N-H···N-type hydrogen bonds found in the solid state structure of quinoline [27], as well as other bulk effects at most only weakly perturb the heavy-atom backbone geometry of the quinoline molecules.

Experimental Section

GED experimental details

Electron scattering intensities for quinoline were recorded at 113(1) °C on reusable Fuji imaging plates by using the above described electron diffractometer and medium temperature nozzle. Acceleration voltage was 60,000(1) V (generating potential), and the primary beam current was about 120 nA. During data acquisition the pressure rose from 7.0×10^{-7} to 8×10^{-6} mbar, and the optimal exposure time was 30–45 s. Table 1 gives experimental details about the datasets used. In Table 2 all independently refined parameters are listed together with the used restraints. Additionally one restraint on a dependent parameter was applied: $r_{6,10} \rightarrow$

1.4154(20) Å, leading to a refined value of 1.415(2) Å. Table 3 gives the independent amplitudes and Table 4 the matrix of parameter correlation.

Computational details

All calculations except the frequency analyses were carried out with the TURBOMOLE program package, version 5.10 [29].

The calculations for the computational levels termed MP2 and SCS-MP2, were performed using the RI-MP2 [30] routine as it is implemented in the ricc2 program deck [31]. For the SCS methods, Grimme's spin-component scaled approach was used in combination with the standard parameters cos = 6/5 and css = 1/3 [32]. TURBOMOLE's def2 basis sets (TZVP, TZVPP, QZVPP) [33] were used throughout in connection with the corresponding auxiliary basis sets for the RI fit [34].

For the calculation of the harmonic force field at B3LYP/6-311G** level of theory [35] GAUSSIAN 03 was used [36]. The programme SHRINK [24] was used to compute harmonic distance corrections and perpendicular curvilinear distance corrections k_{h1}, which in turn were used in the refinement to yield a r_{h1}-type structure (which is an approximation to the equilibrium geometry r_e [7]).

[1] *Die Fragmente der Vorsokratiker. Griechisch und Deutsch von Hermann Diels*, 6th ed., (Ed.: W. Kranz), Weidemann, Hildesheim, **2004**, 57.

[2] W. Friedrich, P. Knipping, M. v. Laue, Interferenz-Erscheinungen bei Röntgenstrahlen. Sitzungsberichte der Mathematisch-Physikalischen Classe der Königlich-Bayerischen Akademie der Wissenschaften zu München, München, **1912**, 303.

[3] H. Mark, R. Wierl, *Naturwiss.* **1930**, *18*, 205.

[4] Groups which are currently active in the field of structure determination of new chemical compounds and maintaining a GED instrument are located in Corvallis, U. S. A. (K. Hedberg), Edinburgh, U. K. (D. W. H. Rankin), Ivanovo, Russia (G. Girichev), Oslo, Norway

(S. Samdal), Moskow, Russia (L. V. Vilkov), Reading U. K. (D. Rice), Tokio, Japan (N. Kuze) and Bielefeld, Germany (N. W. Mitzel). Groups which are currently active in the development of new GED methodologies are in Edinburgh, U. K. (D. Rankin, state specific GED), Pasadena, U. S. A. (A. Zewail, ultrafast electron diffraction), Karlsruhe, Germany (D. Schooss, trapped metal-cluster-ion ED), München, Germany (E. Fill, oriented-molecule electron diffraction).

[5] J. A. Pople, in *From Nobel Lectures, Chemistry 1996 – 2000*, (Ed.: I. Grenthe), World Scientific Publishing Co., Singapore, **2003**, p. 246.

[6] V. J. Klimkowski, J. D. Ewbank, C. van Alsenoy, L. Schäfer, *J. Am. Chem. Soc.* **1982**, *104*, 1476.

[7] D. W. H. Rankin, in *Stereochemical Applications of Gas-Phase Electron Diffraction*, Vol. 1, (Ed.: I. Hargittai and M. Hargittai), VCH-Publishers Inc., New York **1988**, p. 451.

[8] a) A. J. Blake, P. T. Brain, H. McNab, J. Miller, C. A. Morrison, S. Parsons, D. W. H. Rankin, H. E. Robertson, B. A. Smart, *J. Phys. Chem.* **1996**, *100*, 12280; b) P. T. Brain, C. A. Morrison, S. Parsons, D. W. H. Rankin, *Dalton Trans.* **1996**, 4589; c) N. W. Mitzel, D. W. H. Rankin, *Dalton Trans.* **2003**, 3650.

[9] S. L. Hinchley, M. F. Haddow, D. W. H. Rankin, *Dalton Trans.* **2004**, 384.

[10] a) H. Schmidbaur, W. Tronich, *Chem. Ber.* **1968**, *101*, 595; b) N. W. Mitzel, D. H. Brown, S. Parsons, P. T. Brain, C. R. Pulham, D. W. H. Rankin, *Angew. Chem.* **1998**, *110*, 1767; *Angew. Chem., Int. Ed. Engl.* **1998**, *37*, 1670.

[11] K. R. Leopold, M. Canagaratna, J. A. Phillips, *Acc. Chem. Res.* **1997**, *30*, 57.

[12] M. Hagemann, A. Mix, R. J. F. Berger, T. Pape, N. W. Mitzel, *Inorg. Chem.* **2008**, *47*, 10554.

[13] M. Hagemann, R. J. F. Berger, S. A. Hayes, H.-G. Stammler, N. W. Mitzel, *Chem. Eur. J.* **2008**, *14*, 11027.

[14] D. Himmel, N. Trapp, I. Krossing, S. Altmannshofer, V. Herz, G. Eickerling, W. Scherer, *Angew. Chem.* **2008**, *120*, 7914; *Angew. Chem. Int. Ed.* **2008**, *120*, 7772.

[15] N. W. Mitzel, K. Vojinović, T. Foerster, H. E. Robertson, K. B. Borisenko, D. W. H. Rankin, *Chem. Eur. J.* **2005**, *11*, 5114.

[16] N. W. Mitzel, K. Vojinović, R. Fröhlich, T. Foerster, D. W. H. Rankin, *J. Am. Chem. Soc.* **2005**, *127*, 1370.

[17] N. W. Mitzel, C. Lustig, R. J. F. Berger, N. Runeberg, *Angew. Chem.* **2002**, *114*, 2629; *Angew. Chem. Int. Ed.* **2002**, *41*, 2519.

[18] N. W. Mitzel, U. Losehand, A. Richardson, *Organometallics* **1999**, *18*, 2610.

[19] W. Zeil, J. Haase, L. Wegmann, *Z. Instr.* **1966**, *74*, 84.

[20] E. Bauer, *Elektronenbeugung. Theorie, Praxis und industrielle Anwendungen*, Verlag Moderne Industrie, München **1958**, p. 69.

[21] S. Gundersen, S. Samdal, R. Seip, T. G. Strand, *J. Mol. Struct.* **2004**, *691*, 149.

[22] T. G. Strand (Oslo), private communication **2006**.

[23] S. L. Hinchley, H. E. Robertson, K. B. Borisenko, A. R. Turner, B. F. Johnston, D. W. H. Rankin, M. Ahmadian, J. N. Jones, A. H. Cowley, *Dalton Trans.* **2004**, 2469.

[24] V. A. Sipachev, *J. Mol. Struct.* **1985**, *121*, 143.

[25] A. W. Ross, M. Fink, R. Hilderbrandt, in *International Tables for Crystallography*, Vol. C, (Ed.: A. J. C. Wilson), Kluwer, Dordrecht **1992**, p. 245.

[26] H. G. O. Becker, W. Berger, G. Domschkeb, *Organikum*, 22. vollst. überarb. u. aktualis. Auflage, Wiley-VCH, **2004**, p. 40.

[27] J. E. Davies, A. D. Bond, *Acta Crystallogr.* **2001**, *E57*, 0947.

[28] H. Beyer, W. Wolfgang, *Lehrbuch der Organischen Chemie, 21. Aufl.*, Hirzel, Stuttgart, **1988**, p. 628.

[29] a) R. Ahlrichs, M. Bär, M. Häser, H. Horn, C. Kölmel, *Chem. Phys. Lett.* **1989**, *162*, 165; b) M. Häser, R. Ahlrichs, *J. Comput. Chem.* **1989**, *10*, 104.

[30] a) R. Ahlrichs, *Phys. Chem. Chem. Phys.* **2004**, *6*, 5119; b) F. Weigend, M. Häser, *Theor. Chem. Acc.* **1997**, *97*, 331; c) F. Weigend, M. Häser, H. Patzelt, R. Ahlrichs, *Chem. Phys. Lett.* **1998**, *294*, 143; d) F. Haase, R. Ahlrichs, *J. Comp. Chem.* **1993**, *14*, 907.

[31] a) A. Köhn, C. Hättig, *J. Chem. Phys.* **2003**, *119*, 5021; b) C. Hättig, *J. Chem. Phys.* **2003**, *118*, 7751.

[32] S. Grimme, *J. Chem. Phys.* **2003**, *118*, 9095.

[33] a) F. Weigend, F. Furche, R. Ahlrichs, *J. Chem. Phys.* **2003**, *119*, 12753; b) F. Weigend, R. Ahlrichs, *Phys. Chem. Chem. Phys.* **2005**, *7*, 3297.

[34] a) C. Hättig, *Phys. Chem. Chem. Phys.* **2005**, *7*, 59; b) A. Hellweg, C. Hättig, S. Höfener, W. Klopper, *Theor. Chem. Acc.* **2007**, *117*, 587.

[35] a) P. A. M. Dirac, *Proc. Royal Soc. (London)* **1929**, *A 123*, 714; b) S. H. Vosko, L. Wilk, M. Nusair, *Can. J. Phys.* **1980**, *58*, 1200; c) A. D. Becke, *Phys. Rev.* **1988**, *A 38*, 3098; d) C. Lee, W. Yang, R. G. Parr, *Phys. Rev.* **1988**, *B 37*, 785; e) A. D. Becke, *J. Chem. Phys.* **1993**, *98*, 5648.

[36] M. J. Frisch, G. W. Trucks, H. B. Schlegel, G. E. Scuseria, M. A. Robb, J. R. Cheeseman, J. A. Montgomery, Jr., T. Vreven, K. N. Kudin, J. C. Burant, J. M. Millam, S. S. Iyengar, J. Tomasi, V. Barone, B. Mennucci, M. Cossi, G. Scalmani, N. Rega, G. A. Petersson, H. Nakatsuji, M. Hada, M. Ehara, K. Toyota, R. Fukuda, J. Hasegawa, M. Ishida, T. Nakajima, Y. Honda, O. Kitao, H. Nakai, M. Klene, X. Li, J. E. Knox, H. P. Hratchian, J. B. Cross, V. Bakken, C. Adamo, J. Jaramillo, R. Gomperts, R. E. Stratmann, O. Yazyev, A. J. Austin, R. Cammi, C. Pomelli, J. W. Ochterski, P. Y. Ayala, K. Morokuma, G. A. Voth, P. Salvador, J. J. Dannenberg, V. G. Zakrzewski, S. Dapprich, A. D. Daniels, M. C. Strain, O. Farkas, D. K. Malick, A. D. Rabuck, K. Raghavachari, J. B. Foresman, J. V. Ortiz, Q. Cui, A. G. Baboul, S. Clifford, J. Cioslowski, B. B. Stefanov, G. Liu, A. Liashenko, P. Piskorz, I. Komaromi, R. L. Martin, D. J. Fox, T. Keith, M. A. Al-Laham, C. Y. Peng, A. Nanayakkara, M. Challacombe, P. M. W. Gill, B. Johnson, W. Chen, M. W. Wong, C. Gonzalez, J. A. Pople, GAUSSIAN 03 (revision E.01) Gaussian, Inc., Wallingford CT, (U. S. A.) **2004**.